Title

Whispering gallery mode emission from dye-doped polymer fiber cross-sections fabricated by near-field electrospinning

Journal

Nanoscale, 12(17)

ISSN

2040-3364

Authors

Cheeney, Joseph E

Hsieh, Stephen T

Myung, Nosang V

et al.

Publication Date

2020-05-07

DOI

10.1039/d0nr00147c

Peer reviewed

Citation: *Nanoscale*, 2020,12, 9873-9883

Whispering Gallery Mode Emission from Dye-Doped Polymer Fiber Cross-sections Fabricated by Near-Field Electrospinning

Joseph E. Cheeney,[a,‡] Stephen T. Hsieh,[a,‡] Nosang V. Myung,[b] and Elaine D. Haberer*[,a,c]

[a]Materials Science and Engineering Program, University of California, Riverside, CA 92521

[b]Department of Chemical and Environmental Engineering, University of California, Riverside, CA 92521

[c]Department of Electrical and Computer Engineering, University of California, Riverside, CA 92521

*Corresponding author email: **haberer@ucr.edu**

ABSTRACT: Whispering gallery mode (WGM) resonators demonstrate great potential for photonic and sensing applications. Yet, these devices are often disadvantaged by costly materials or complex fabrication approaches, in addition to lack of manufacturing scalability. Near-field electrospinning (NFES), a recently emerged facile fiber fabrication method, offers a solution. Here, WGM resonances are reported in Rhodamine 6G-doped poly(vinyl) alcohol (PVA) microfibers via NFES. Diameters are tuned over a range of more than 10 μm by varying substrate stage speed. Fibers display uniform distribution of dye, smooth surfaces, and circular cross-sections, all critical for supporting WGMs. High quality (Q) resonances are confirmed within fiber cross-sections through polarization experiments, free-spectral range analysis, and Mie-theory-derived mode assignment. In addition to WGMs, groups of associated spiral or conical modes are observed due to taper-induced weak optical confinement along the fiber axis. Crosslinked, dye-doped PVA fibers are utilized to sense the ethanol concentration in ethanol-water mixtures and actuation mechanisms are evaluated by comparison to theoretical spectra. The demonstration of high-Q resonances within NFES polymer microfibers is a critical step toward simple, cost effective, high-volume fabrication of WGM resonators for optoelectronics and biomedical devices.

1. Introduction

Among the highest quality (Q) optical cavities, whispering gallery mode (WGM) resonators have unique potential to address critical challenges in both optoelectronics and healthcare. These mirrorless structures display strong optical confinement due to total internal reflection at the cavity periphery. Their radial symmetry allows light to recirculate numerous times, enabling enhanced light-matter interactions. WGM resonances are essential to many important photonic devices including low-threshold lasers,[1–5] frequency combs,[6–8] and waveguides[9] as well as in sensing applications such as bulk chemical sensors,[4,10–14] label-free biosensors,[15–17] single ion detectors,[18] and mechanical deformation indicators.[19–21]

A wide variety of materials including glass,[15,22,23] semiconductors,[24–29] and polymers[1,2,30,31] have been used to make WGM resonators. Among these, polymer-based WGM

cavities offer reduced material costs, simple processing strategies, and straightforward incorporation of a variety of emitters. A range of polymer cavity geometries and fabrication techniques have been explored from drop casted spheres[31] to lithographically-defined conical structures[2] to inkjet-printed, wedge-shaped microdisks.[32] Of the many reports of WGM polymer cavities, only a limited number focus on fibers. Hollow fiber resonators have been fabricated from dye-doped polymethylmethacrylate (PMMA) preforms using heat drawing. These free-standing polymer fibers, which were 100s of microns in diameter, demonstrated both directional emission[33] and thermo-optic tuning of WGMs.[34] In addition, PMMA/epoxy resin fibers have been manually drawn directly from solution using a sharp metal tip to create WGM microlasers and refractive index based optical sensors.[1,6] Furthermore, arrays of PMMA/epoxy resin microfibers, embedded in PDMS were produced via spiral drawing.[35] In this process, the substrate served as a spool that rotated and translated via precise motor control. These dye-doped polymer fiber lasers exhibited sensitivity to strain and force perturbations. While these polymer fiber processing methods are comparatively simple and inexpensive, they lack manufacturing scalability.

One promising technique for high-volume, rapid manufacturing of polymer fiber WGM cavities is electrospinning, also known as far-field electrospinning. This method can be used to fabricate diverse morphologies and structures including simple homogeneous, bead-like, porous, hollow, and coaxial core-shell polymer fibers, among others.[36] A straightforward apparatus pumps a polymer solution through a hypodermic needle typically positioned 10s of centimeters from the substrate (or collector). A voltage applied between the needle tip and collector draws the solution from the needle, forming a liquid jet and depositing fibers on the collector with an unstable, whipping motion. Far-field electrospinning has been used to fabricate a handful of optically active resonators used as lasers[37–40] and organic solvent vapor sensors.[41] Reports

include dye-doped polymer fibers which support Fabry-Perot modes along their length[39] and 3-D resonances within their non-circular cross-sections.[37] In addition, ring resonators with sub-wavelength cross-sections[38,41] have been formed from random networks of electrospun nanofibers and bottle micro-resonators have been generated from microdroplets of polymer gain medium deposited on electrospun fibers.[40] While far-field electrospinning can rapidly produce many fibers, because the chaotic whipping motion far from the needle tip dominates fiber deposition it lacks the spatial precision necessary for many applications. Recently, a similar technique known as near-field electrospinning (NFES) has emerged.[42] This electric-field-driven approach combines the production scale of electrospinning with direct-write patterning by reducing the tip-to-collector distance from 10s of centimeters to a few millimeters or less. The lower tip-to-collector distance uses the straight, stable jet that forms near the tip, avoiding the instabilities and whipping which occur at greater distances. Notably, NFES has demonstrated the precision and control required to fabricate well-organized fiber meshes,[43] as well as to suspend fibers between posts just a few tens of microns in diameter.[44] Typically, the polymer fibers produced by NFES are approximately 10s to 100s of nanometers in diameter, too small to support high quality WGMs within their cross-sections.

In this work, we investigated NFES of micron-scale, dye-doped poly(vinyl) alcohol (PVA) fibers, and the high Q optical resonances supported by their smooth, circular cross-sections. PVA is a versatile water-soluble polymer which has been used in textile, biomedical and optical applications.[45–47] For aqueous-based applications, it can be crosslinked to form an insoluble hydrogel.[48,49] Sizeable weight percent solutions of PVA were used in conjunction with reduced stage speeds to direct write suspended fibers approximately 3 to 18 μm in diameter. The emission from these slightly tapered, optically active resonators revealed groups of sharp peaks ascribed to a combination of WGMs and spiral or conical modes. The longest wavelength peak

within each group was identified as an in-plane WGM using mode polarization, Mie theory-based mode assignment, and free spectral range (FSR) measurements over a range of diameters. WGM quality factors of nearly 14,200 were observed for larger fiber diameters. These water-soluble PVA fibers were subsequently crosslinked via glutaraldehyde to impart stability and preserve cavity geometry for aqueous-based sensing. As a result, the maximum measured WGM cavity Q increased to approximately 19,800. As a model analyte system, the fibers were submerged in a range of ethanol-water mixtures and the corresponding WGM resonance shifts were measured as ethanol concentration was increased. Theoretical spectra were used to investigate sensing mechanisms by estimating the changes in fiber diameter and optical mode effective refractive index associated with the observed wavelength shifts. The success of NFES, a potentially low-cost, large-scale manufacturing technique, in producing micron-sized fibers that support WGMs and are highly sensitive to environmental changes is an important step toward the scalable production of affordable chemical sensors and biosensors.

2. Experimental Details

2.1 Fabrication and Characterization of Electrospun Polymer Fibers

PVA (M_W: 13,000-23,000 g mol^{-1}, 98% hydrolyzed, Sigma Aldrich) and Rhodamine 6G (R6G, Sigma Aldrich) were dissolved in deionized water and mixed with a magnetic stir bar in a hot water bath at 80°C for 2 h to obtain a homogeneous 25 wt%, 0.0035 gPVA/gR6G solution. The mixture was cooled for 1 h under ambient conditions and physicochemical properties were measured including viscosity (LV DV-I Prime, Brookfield), surface tension (DuNouy Interfacial Tensiometer, Central Scientific Co. Inc.), and conductivity probe (Vernier). Optical absorbance (Cary 500, Varian), fluorescence (QM-400, Horiba), and ellipsometry (UVISEL Spectroscopic)

measurements were performed on spin coated thin films of the PVA/R6G solution. Ellipsometry was carried out at 45 ± 5% humidity.

The dye-doped polymer solution was loaded into a 1 mL syringe and pumped through a 27-gauge blunt-tip needle at a rate of 10 μL h^{-1} using a syringe pump (NE-1010, New Era). A high voltage source (NO3.5HP8.5, Acopian) was used to apply a 2 kV to the needle tip. A glass substrate of dimensions 15 x 15 x 1 mm was used as the collector and was placed on top of an X-Y stage (A-LSQ300D, Zaber) programmed to move in a parallel-line pattern. The substrate was scribed with lines perpendicular to the intended fiber deposition direction to allow fibers to be suspended. Approximately 1 cm long fibers were written 200 μm apart from each other. The needle tip-to-collector (T-t-C) distance was fixed at 1.25 mm, while the stage speed was varied from 0.1-10 mm s^{-1}. Electrospinning occurred under ambient temperature, pressure, and humidity. Electrospun fiber diameters were characterized using a digital optical microscope (KH-7700, Hirox) with a 35x objective and built-in measurement software. Fiber surface roughness was measured using tapping mode atomic force microscopy (AFM, Dimension Edge, Bruker) and a silicon tip. For cross-sectioning, the ends of the fibers were glued to the substrate, immersed in liquid nitrogen, and the substrate was broken along a scribe mark. While still in liquid nitrogen, the samples were placed in a vacuum desiccator for 24 h to prevent condensation from forming on the fibers. For use in scanning electron microscope (SEM; Vega3, Tescan), fibers were coated with a thin gold layer prior to characterization of fiber morphology, surfaces, and cross-sections. Confocal fluorescence microscopy (SP5, Leica Microsystems) was also used to image the dye-doped fibers.

2.2 Crosslinking Fibers

For aqueous applications, the water-soluble PVA fibers were chemically crosslinked with glutaraldehyde to make them water-stable. A three-step process, derived from previous reports, was used to crosslink the PVA fibers while still maintaining the ability to support WGMs.[50,51] Briefly, the fiber ends were glued to the substrate, placed in a closed chamber, and simultaneously exposed to vapor from a 1 M HCl solution and a 50% glutaraldehyde solution for 24 h. Next, the fibers were exposed to vapor from a 5 M HCl solution and a 50% glutaraldehyde solution for 24 h. For the last step, the fibers were submerged in a 50% glutaraldehyde solution for 24 h, rinsed thoroughly with water, and allowed to dry.

2.3 Optical WGM Measurement and Sensing

A laser confocal system (LabRam, Horiba Scientific) in a microphotoluminescence (μPL) configuration was used to evaluate the dye-doped PVA fiber WGM resonators. A single fiber was optically excited with 1 μW from a 532 nm CW laser (Ventus, Laser Quantum) focused to a spot size of approximately 3 μm using a 50x objective (NA = 0.75). Resonator emission was collected with the same objective, directed through a longpass filter (> 532 nm), and analyzed using a charge-coupled device (CCD) spectrometer with an 1800 lines mm^{-1} grating and a spectral increment of around 0.014 nm. WGM Q factors were analyzed by fitting each peak with a Lorentzian function. For ethanol-water sensing experiments, the sample was submerged in a pool of water in which the ethanol concentration was varied from 0 to 30% by volume while keeping the total solution volume constant. Spectra were collected in 3 min intervals. The laser was shuttered between measurements to prevent photothermal effects and minimize bleaching. A 50x long-working-distance (NA = 0.50) objective was used, and the excitation power was increased to 2 μW.

To determine important WGM parameters and azimuthal mode numbers, theoretical spectra were obtained by using a Mie-theory derived approximation[52]

$$\lambda \cong \pi n_{host} D \left[\nu + \frac{\alpha_s \nu^{\frac{1}{3}}}{2^{\frac{1}{3}}} - \frac{P}{\left(n_{eff}{}^2 - 1\right)^{\frac{1}{2}}} + \frac{3}{10} \frac{\alpha_s{}^2}{2^{\frac{2}{3}} \nu^{\frac{1}{3}}} - \frac{P\left(n_{eff}{}^2 - \frac{2P}{3}\right)}{\left(n_{eff}{}^2 - 1\right)^{\frac{3}{2}}} \frac{\alpha_s}{2^{\frac{1}{3}} \nu^{\frac{2}{3}}} \right]^{-1} \quad (1)$$

where D is resonator diameter, ν is the mode number + 0.5, α_s are the roots of the Airy function, n_{eff} is the effective refractive index of the resonance, and $P = 1/n_{eff}$ for TM and n_{eff} for TE modes, respectively. The refractive index of the surrounding medium (n_{host}) was taken as either 1.000 for fibers in air or was based on literature measurements for ethanol-water concentrations[53] (shown in Figure S1), with values ranging from 1.3325 to 1.3494. Equation (1) was evaluated by incrementally varying D, n_{eff} and azimuthal mode number. Solutions were compared to fluorescence spectra obtained from the WGM fibers, and the least mean residual squared was taken as the best fit. The range of input D and n_{eff} values used to determine best fit corresponded to optical images and ellipsometry measurements, respectively. For sensing of ethanol-water mixtures, measurements made within 5 min of ethanol addition were disregarded due to transient behavior and the mode number was constrained despite changing ethanol-water concentrations.

3. Results and Discussion

3.1 Near-Field Electrospinning of Dye-Doped Polymer Fiber Resonators

Solutions for NFES of optically active, fiber resonators were prepared by combining R6G with PVA. A relatively high weight percent PVA was used to spin fibers. Typically, increasing polymer weight percent increases viscosity and conductivity while reducing surface tension, all of which contribute to the fabrication of larger fibers.[36,54] Because they are critical in manipulating electrospun fiber diameter, the physicochemical properties of these solutions were measured. The

surface tension, electrical conductivity, and viscosity were 56 ± 1 dynes cm^{-1}, 2726 ± 102 μS cm^{-1}, and 717.5 ± 73.8 cP, respectively. For the purpose of optical characterization, this dye-doped polymer solution was spin-coated onto a glass slide, forming an approximately 5 μm thick film. The absorbance and emission spectra of the R6G-PVA film were measured and are shown in Figure 1. Peak absorbance and emission wavelengths were 537 nm and 548 nm, respectively. Minimal spectral overlap of absorbance and emission was observed for wavelengths greater than 575 nm. As measured by ellipsometry at 45 ± 5% humidity, the average refractive index, *n*, of the R6G-PVA films between 580 and 700 nm was $n = 1.464 \pm 0.006$.

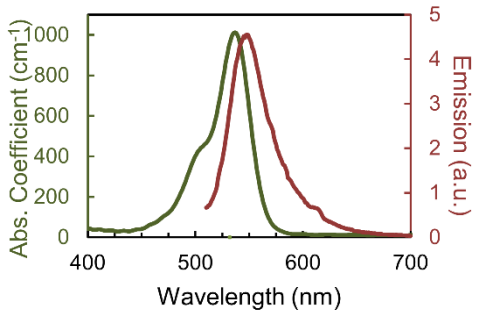

Figure 1. Absorption and emission spectra of spin-coated R6G-PVA thin film.

The NFES system used to fabricate fiber-based optical cavities is illustrated in Figure 2a. The polymer solution was pumped through a syringe and fed through a hypodermic needle, forming a droplet. An applied voltage between the needle (tip) and substrate (collector) allowed the polymer solution to overcome its surface tension, generate a Taylor cone, and induce fiber formation. Fiber was deposited on the collection substrate as the computer-controlled stage scanned in a programmed parallel-line pattern composed of lines 1 cm in length, spaced approximately 200 μm apart. With these dimensions, 10s of fibers were written on a single substrate. Electrospinning of the R6G-PVA solution is depicted in Figure 2b. Microscale polymer

fiber was drawn from the droplet in the scan direction. As shown in Figure 3a, fiber diameter was dependent on stage speed. Optical images of fibers for each electrospinning condition, in addition to histograms of fiber diameter, are shown in Figures 3b-e and S2, respectively. Using a scan rate of 10 mm s^{-1} the average fiber diameter was 2.8 ± 1.3 μm, whereas a reduced stage speed of 0.5 mm s^{-1} increased the average diameter to 12.4 ± 5.9 μm. Thus, average fiber size was adjusted by more than a factor of 4. Scan velocity can control the degree of mechanical drawing of the polymer solution during spinning, greatly influencing fiber diameter.[44,55] Similar trends have also been observed for stage speeds 2 to 40 times larger than used in these studies.[44,55–57] The combination of electrospinning parameters (e.g. solution, pattern dimensions, etc.) used here approached the spatial limitations of our apparatus and controller. As a result, scan rate affected pattern fidelity with write deviations increasing at higher speeds, particularly near end points. The use of rather viscous, high weight percent polymer solution and reduced stage speed enabled fabrication of larger fibers. The sizable diameters generated by a 0.5 mm s^{-1} stage speed were compatible with observation of high quality WGMs, therefore fibers electrospun with these conditions were selected for further study.

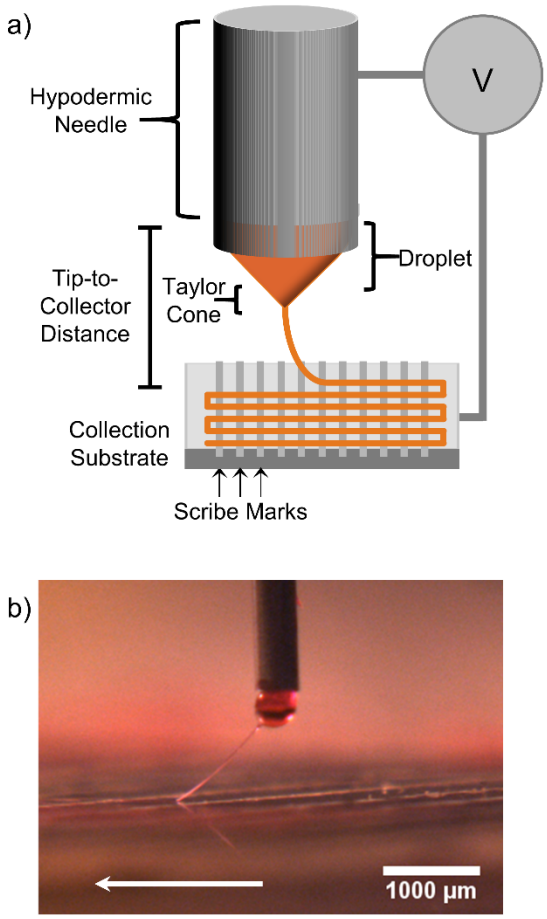

Figure 2. a) Schematic of near-field electrospinning (NFES) apparatus showing deposition of suspended polymer microfibers. b) Optical image of Taylor cone formation and fiber drawing from polymer droplet during NFES process. The arrow indicates the direction of stage motion.

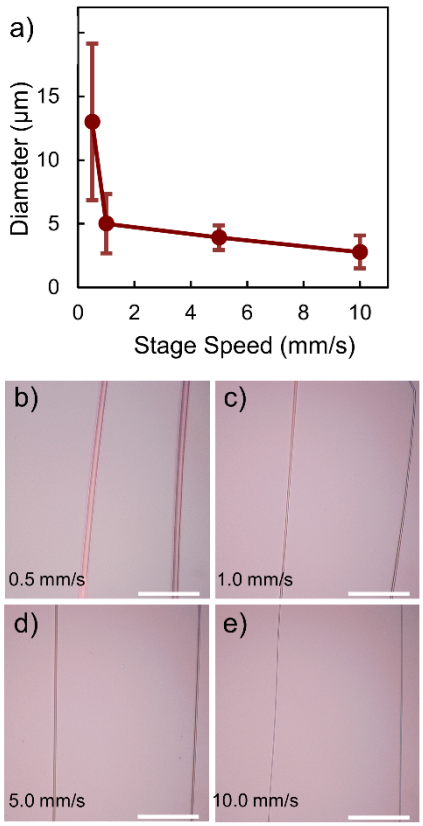

Figure 3. R6G-PVA electrospun fiber a) diameter and b)-e) optical images as a function of stage speed. Average fiber diameter increased as scan rate decreased. Average and standard deviation were determined from >85 measurements. Scale bars: 100 μm.

Using a scan rate of 0.5 mm s^{-1}, R6G-PVA fibers were electrospun on a glass substrate. Prior to electrospinning, 5-10 scribe marks were made in the substrate perpendicular to the fiber deposition direction as previously indicated in Figure 2a. These nearly 20 μm deep trenches prevented optical coupling of resonator-supported-modes to the underlying glass substrate. Figure 4a and 4b show the fluorescence emission and an SEM image of electrospun dye-doped polymer fibers suspended across a scribe mark, respectively. R6G fluorescence was relatively uniform throughout the fibers, without evidence of substantial dye molecule agglomeration. In addition, no fiber sagging or drooping was observed. Higher magnification electron microscope images, shown in Figure 4c and 4d, revealed smooth fiber surfaces without significant striations or ridges.

A root-mean-squared roughness of 2.4 nm was measured via atomic force microscopy (Figure S3). Moreover, fiber cross-sections produced with the freeze-snap technique were circular, and void of flat regions or significant distortions in shape, as shown in Figure 4e. These fibers were an enhancement upon a previous report of similarly sized electrospun polymer fiber resonators which yielded rough, non-circular structures.[37] As revealed in Figure S4, fiber diameter was found to vary gradually with length, and no bead-like structures were observed. More than 15 fibers, with over 200 μm in length analyzed on each, indicated an average diameter change of 0.037 ± 0.034 μm per micron of fiber length.

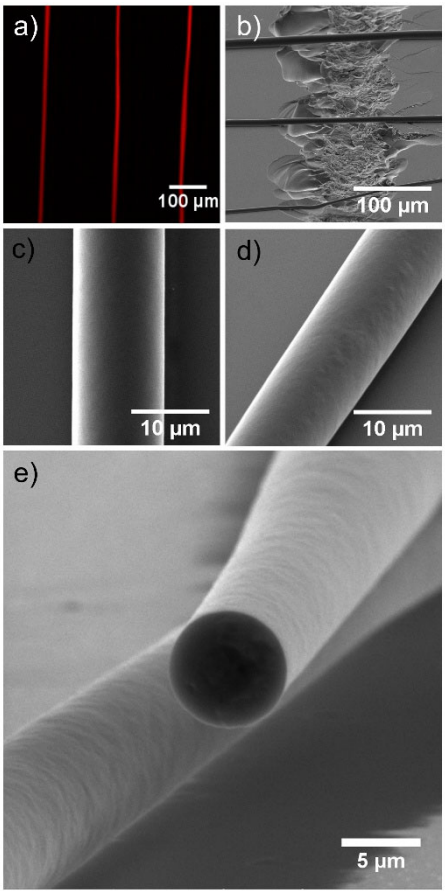

Figure 4**.** a) Fluorescent emission and b-e) representative SEM images of PVA fibers electrospun with a stage speed of 0.5 mm s^{-1} and a R6G/PVA mass ratio of 0.0035.

3.2 Whispering Gallery Mode Detection and Characterization

Emission from the R6G-PVA fiber optical cavities was measured using a μPL set-up with a coherent, continuous wave (CW) 532 nm excitation source and an approximately 3 μm spot size. Excitation power dependent measurements from 5 nW to 50 μW indicated that the resonators were in the spontaneous emission regime. The higher excitation power failed to produce lasing, likely due to the insufficient photostability of fluorescent dye.[58] Consequently, to minimize dye bleaching, yet ensure an adequate signal-to-noise ratio, 1 μW of excitation power was used. Figure 5a shows a representative spectrum of a single, as-spun dye-doped PVA fiber with a measured diameter of 4.2 μm. The investigation focused on wavelengths greater than 575 nm due to the minimal overlap in R6G absorbance and emission within this spectral region. Paired groups of sharp resonances were observed to decorate the broad fluorescence emission of R6G. The WGM resonance condition is:

$$m\lambda = \pi D n_{eff} \quad (2)$$

where m is an integer, λ is the wavelength, D is the resonator diameter, and n_{eff} is the effective refractive index. The groups of closely spaced modes were attributed to WGMs supported within the fiber cross-section, in addition to spiral or conical modes with finite longitudinal components and wavelengths slightly smaller than WGM resonance.[59–61] Variations in fiber geometry including both bottle structures[62,63] and tapers[64,65] can facilitate the observed optical confinement. In particular, the aforementioned diameter changes were likely contributors. To further investigate the groups of closely spaced modes, emission was collected along the length of the fiber in 0.8 μm increments (Figure S4). Within each spectrum, the dominant intensity peak was dependent on measurement location. As the excitation and collection optic was scanned along the

fiber length, resonance features emerged and faded within a short distance, typically < 10 μm, indicating fairly compact mode localization. Previous reports[59,60] attribute this form of mode localization to conically-shaped fibers that confine light via a reflection process on the smaller diameter side and a self-interference process on the larger diameter side. Additional electrospinning process development is required to more precisely control fiber diameter, and further suppress longitudinal resonance components.

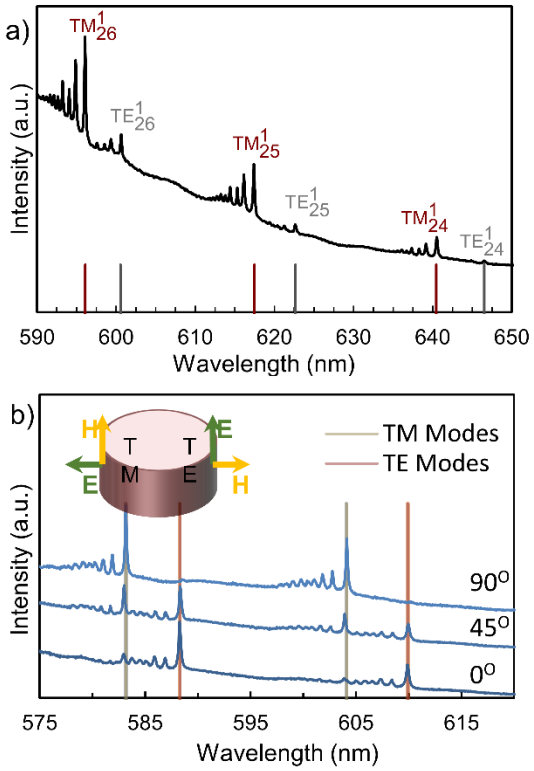

Figure 5. a) Spectrum of 4.2 μm diameter dye-doped, electrospun PVA fiber. Broad fluorescence emission was decorated by groups of sharp peaks. Mie theory was used to identify first order TE and TM WGMs. b) Spectra of a 4.7 μm diameter fiber taken with a polarizing filter to establish the polarization of the resonances. At 0° the polarizer is parallel to fiber axis while at 90° the polarizer is perpendicular. Inset: E and H field vector orientation associated with TM and TE modes.

To distinguish modes with similar electromagnetic field oscillation, a polarizer was placed between the fiber and the monochromator. Representative polarization-dependent spectra are shown in Figure 5b. Here, modes with the electric field vector perpendicular to the resonator surface are transverse magnetic (TM) and modes with the electric field vector parallel to the length of the fiber are transverse electric (TE). As demonstrated, within a group, all the peaks were the same polarization. The shorter and longer wavelength groups were TM and TE, respectively.

Having identified the peak pairs as TE and TM WGM modes, theoretical spectra were calculated using an asymptotic formula for resonance and mode identification based on Mie theory.[52] The position of the highest intensity peak within each group was compared to the corresponding theoretical peak value, and the best fit was determined by the least sum of the residuals squared. Resonances were assumed to be first order radial WGMs, as these are typically the lowest loss modes. Mode assignments in Figure 5a correspond to a diameter of 4.5 μm and n_{eff} of 1.3080 (TE) and 1.239 (TM). Because TM and TE modes penetrate the surrounding environment to different degrees, a small difference in n_{eff} values was expected.

As illustrated in Figure 6a, the longest wavelength peaks, associated with in-plane WGM resonances, from two successive groups within the same polarization were used to determine free spectral range (FSR). The spacing between consecutive modes was expected to decrease with increasing cavity length as defined by:

$$FSR = \frac{\lambda^2}{Ln_{eff}} \quad (3)$$

where L is the resonator path length. For WGMs, the cavity circumference, πD, is nominally the path length. FSR is plotted versus fiber diameter in Figure 6b for dye-doped electrospun fibers

ranging from 3 to 18 μm in size. The inverse relationship between FSR and *D* (as emphasized by the solid curve), is characteristic of WGMs and further excludes both Fabry-Perot resonances[37] along the fiber length and random cavity resonances.[38,39] Cavity Q-factors, defined as:

$$Q = \frac{\lambda_{Resonance}}{\lambda_{FWHM}} \quad (4)$$

were evaluated for several optical cavities by fitting each peak with a Lorentzian function. A single high Q peak (~14,200) with a 0.044 nm FWHM is represented in Figure 6c and measured Q values for a range of as-spun fiber diameters are shown in Figure 6d. Given the relatively weak dependence of Q factor on diameter, radiative losses were not dominant, but rather material absorption or surface scattering were considered the main limitations on resonator performance.[66–68] Compared to other similarly sized polymer fibers, the near-field electrospun WGM fiber resonators described here possessed higher Q-factors. As example, ~10 μm diameter manually drawn dye-doped PMMA/epoxy fibers have been reported with Q-factors near 6500[1]. Similarly, a Q-factor of 1942 has been measured for an 11.7 μm far-field electrospun dye-doped PMMA fiber[69]. Notably, unlike the WGM fiber resonators studied here, both reports were under lasing or hot cavity conditions with significant linewidth narrowing.

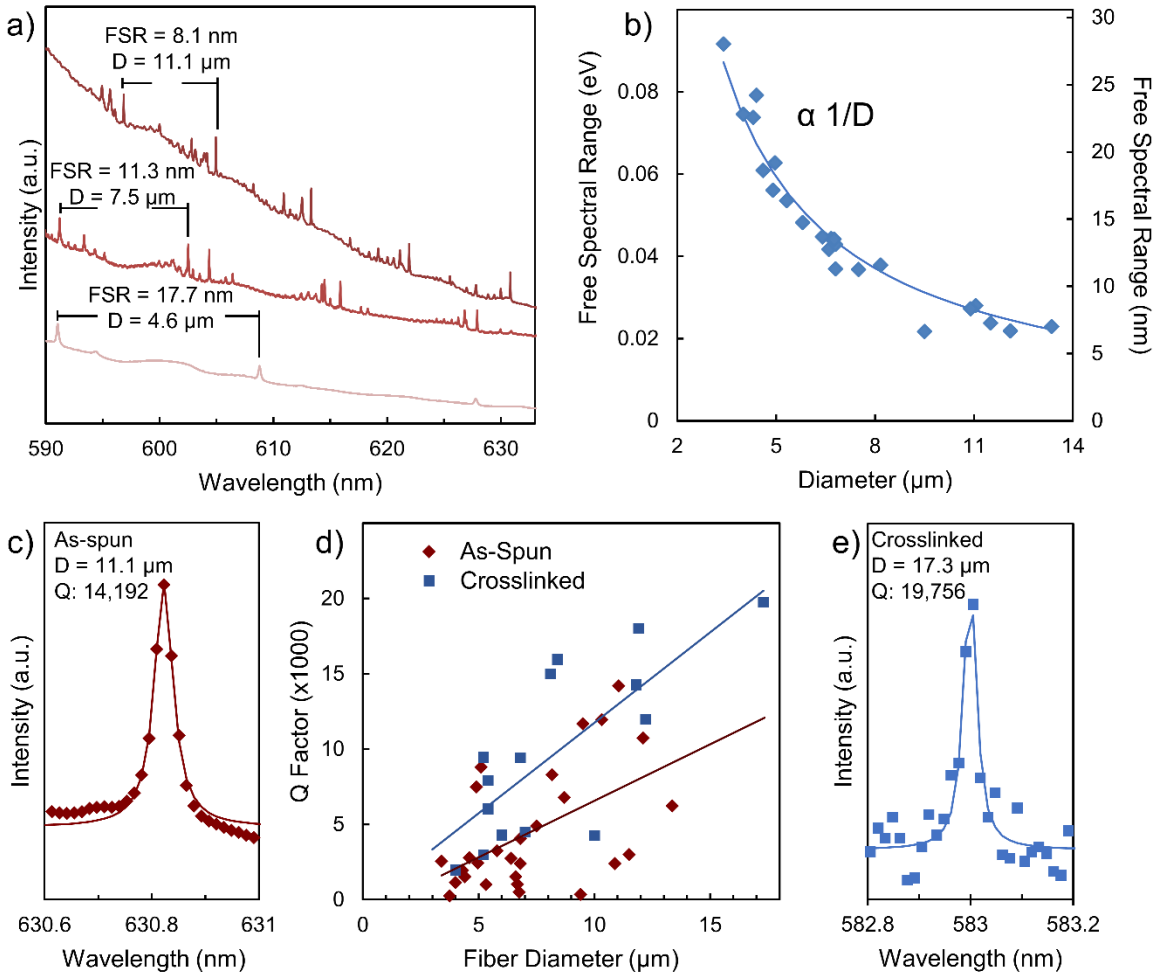

Figure 6. a) Emission spectra of three different fiber diameters with free spectral range (FSR) measured between the longest wavelength peaks from successive groups within the same polarization. Emission intensity is offset for clarity. b) FSR plotted as a function of fiber diameter. FSR was proportional to 1/D as denoted by the solid line. c) A high Q mode associated with the as-spun 11.1 μm diameter fiber in part a) with a Lorentzian curve fit. d) Q-factor plotted versus diameter for as-spun and crosslinked fibers. Q values approaching 14,200 for as-spun fibers and nearly 19,800 for crosslinked fibers were recorded for larger diameters. e) A high Q mode associated with a 17.3 μm diameter crosslinked fiber with a Lorentzian curve fit.

A three-step glutaraldehyde treatment based, in part, on previous reports[50,51] was used to crosslink dye-doped PVA fibers, rendering them insoluble in aqueous solution. As shown in Figure S6, after crosslinking, there was an approximately 13% increase in average fiber diameter and some fiber curvature developed (Figure 7a). This was likely due to swelling and/or polymer

relaxation associated with the water-based crosslinking process. Nonetheless, as demonstrated in Figure S7, after immersion in water for 24 h, glutaraldehyde-treated PVA fibers were unchanged and no additional swelling or distortion in shape was observed. The photoluminescence of the crosslinked fibers was measured in air. As described in Figure 6d and 6e, after glutaraldehyde treatment, Q factors increased overall, attaining a value near 19,800 for one of the larger diameter fibers. Further studies are necessary to fully understand this phenomena, but it is believed that the crosslinking process may reduce fiber surface roughness and the associated scattering losses via solvent-vapor surface smoothing.[70]

3.3 Ethanol-Water Sensing

WGM resonators have shown great utility as chemical and biological sensors.[1,6,15] Electrospun R6G-PVA micro-fibers were assessed as chemical sensors using ethanol in water as a model system. A crosslinked WGM fiber resonator was placed in a water bath, as in Figure 7a, and optical spectra were collected. Notably, once submerged, resonance wavelengths were invariant in the water bath (Figure S8), thus supporting optical microscopy evidence that the crosslinked PVA fibers were water stable, and that heating effects were minimal. Q values of the submerged fibers shrunk by roughly a factor of 9 and FSR decreased slightly due to the sizable reduction in refractive index difference between the cavity and its surroundings. For ethanol-water sensing, the concentration of ethanol was increased in 10% (v/v) increments. As shown in Figure 7b, a corresponding red-shift in WGMs resonant wavelength was associated with each increase. The resonant wavelength of the mode initially observed at 613.5 nm was plotted as a function of time in Figure 7c. Immediately after each addition of ethanol, the resonant wavelength rapidly increased, and then plateaued. Evaporation losses at higher ethanol concentrations resulted in small, but discernable blue shifts at longer measurement times. Figure 7d depicts the resonance

wavelength of the same peak versus ethanol concentration. The spectral response of the resonator was linear within the range of ethanol concentrations measured, resulting in a sensitivity of 0.1133 nm/%. As demonstrated in Figure S9, the sensitivity of the cavity to ethanol concentration was wavelength dependent, due to decreased light confinement at longer wavelengths. Using the relationship between refractive index and ethanol concentration found in Figure S1[53], the measured sensitivities were comparable to those of other polymer-based WGM resonators. As an example, dye-doped PMMA/epoxy resin fibers[6] had a sensitivity of approximately 0.1391 nm/%. Similarly, hollow PMMA fibers embedded with a dye-doped microrings[71] demonstrated sensitivities near 0.1245 nm/%.

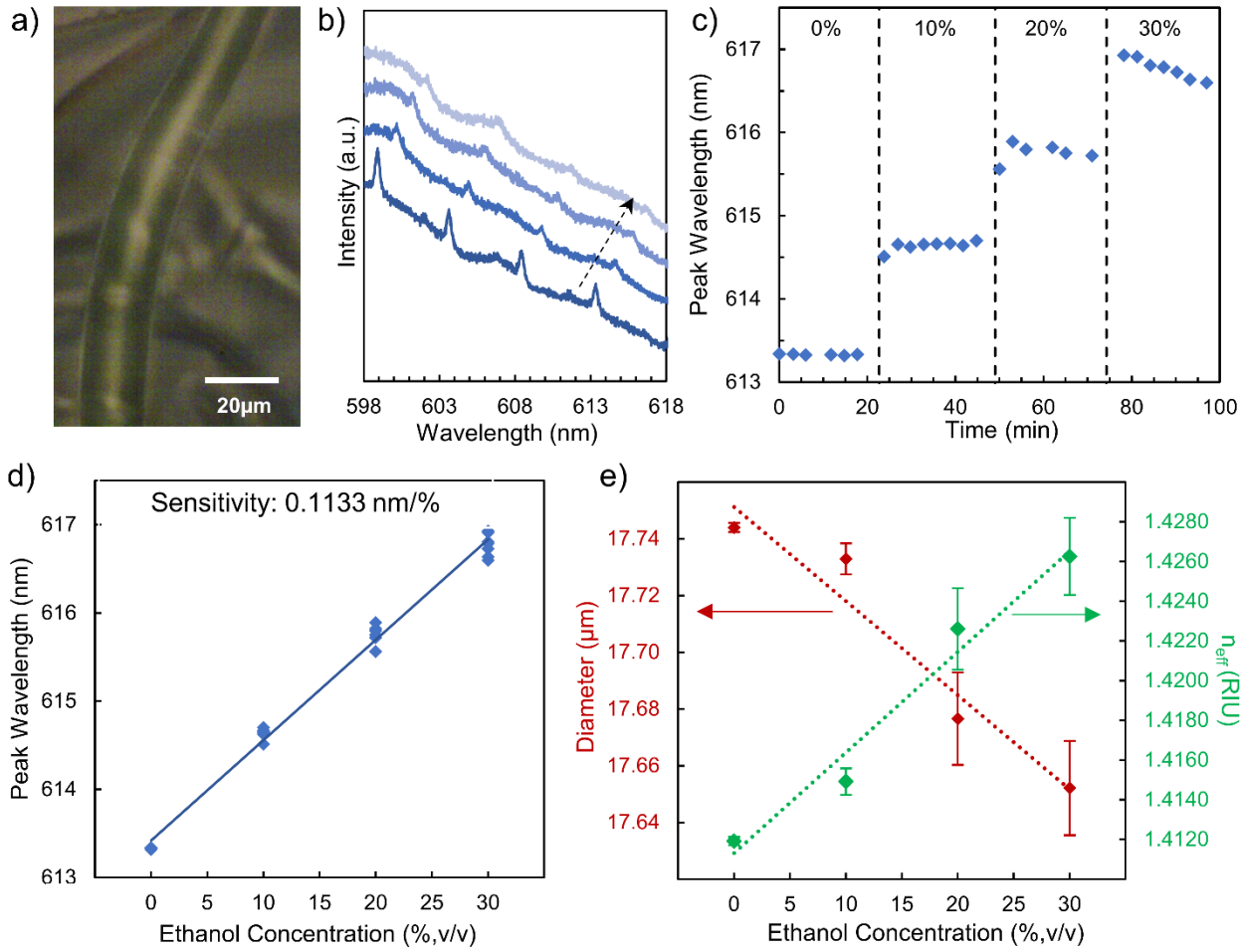

Figure 7. a) A 15.9 μm diameter WGM fiber sensor submerged in a water bath. b) Fluorescence spectra of fiber resonator in 0%, 10%, 20%, and 30% (v/v) ethanol-water solution. Arrow indicates increasing ethanol concentration. Emission intensities are offset for clarity. c) Peak emission wavelength of the mode initially observed at 613.5 nm as a function of time. A red-shift in WGM resonance was observed for each increase in ethanol concentration (as denoted by dashed, vertical lines). d) Peak emission wavelength as a function of ethanol concentration. The calculated sensitivity within this linear performance region was 0.1133 nm/%. e) Calculated resonator diameters and effective refractive indices with increasing ethanol concentration; fiber diameters shrunk slightly, while n_{eff} increased. Each data point represents the average fitted diameter or n_{eff} obtained.

Both volumetric and effective refractive index changes can contribute to WGM wavelength shifts and sensor performance. The relationship between resonance shift and these mechanisms can be expressed by

$$\frac{\Delta\lambda}{\lambda} = \frac{\Delta n_{eff}}{n_{eff}} + \frac{\Delta D}{D} \quad (5)$$

Due to the evanescent field associated with WGMs, the effective refractive index depends on both n_{cavity} and n_{host}. Unlike inorganic optical resonators, the addition of solute can cause changes in the n_{cavity} of polymer cavities through solute uptake, as well as n_{host}. Furthermore, solute uptake can be accompanied by resonator dimensional changes. Indeed, other WGM polymer-based cavities have demonstrated the combined influence of environmental refractive index, solvent uptake, and/or cavity expansion or contraction on sensor response[41,72–75]. When exposed to alcohol vapors, both swelling and vapor uptake caused redshifts in resonances of random optical networks of poly(methyl methacrylate) (PMMA) fibers[41]. Similarly, interaction of volatile organic compounds with PDMS-coated SiO_x quasi-toroidal ring resonators resulted in a redshift which could be parsed in to contributions from polymer swelling and an increase in n_{cavity}[74]. Additionally, solvent penetration and swelling were observed for WGMs in polystyrene microbeads immersed in alcohol solutions, although changes in n_{host} dominated sensor performance[75].

To understand the transduction mechanisms associated with the crosslinked, dye-doped PVA WGM fibers, the sensing spectra were examined using Equation (1), a Mie theory-based asymptotic formula, to extract best fit values for D, n_{eff}, and azimuthal mode number. Similar Mie theory approaches have been used to account for dimensional and refractive index changes associated with humidity, or adsorbed polyelectrolyte and biomolecule layers[73,76,77]. The average best fit diameters and effective refractive indices for all sensing spectra as a function of ethanol concentration are shown in Figure 7e. As the ethanol concentration increased from 0 to 30%, the calculated D shrank approximately 90 nm or just 0.5%. The reduction in diameter is consistent with reports of highly crosslinked PVA hydrogels with a large degree of hydrolysis in ethanol-water solvent mixtures[78–80]. Conversely, n_{eff} increased with ethanol concentration. As the refractive index of ethanol is larger than water, depending on the extent of fiber uptake, both n_{host}

and n_{cavity} could contribute to this increase. The resonance peak is expected to blue-shift as fiber diameter shrinks and red-shift as n_{eff} increases. As a net red-shift was observed with increasing ethanol concentration, the sensing performance of the WGM fiber was dominated by an effective refractive index change rather than dimensional change.

3. Conclusion

To conclude, NFES was used to fabricate R6G-PVA fibers that supported WGM resonances within their cross-sections. This readily scalable, direct-write technique allowed for precise, patterned deposition of several centimeters of fibers on each substrate. By utilizing a relatively high weight percent polymer solution and stage speeds much slower than other NFES reports,[44,55–57] fiber diameters were tuned into the micron range while maintaining smooth surfaces and circular cross-sections. The broad fluorescence emission of these fibers was decorated by groups of high Q peaks. These resonances were ascribed to WGMs which circulated around the fiber circumference, as well as spiral or conical modes with small longitudinal components and slightly smaller wavelengths. Additional studies are needed to minimize axial components and simplify the spectra of these optically active resonators. For aqueous applications, R6G-PVA fibers were crosslinked with a glutaraldehyde treatment. This process caused fiber diameters to swell and cavity Q to increase, likely due to solvent-vapor smoothing of the fiber surface. Despite emission spectrum complexity, chemical sensing of the ethanol-water system exhibited a sensitivity of 0.1133 nm/%. NFES of dye-doped polymer microfiber WGM resonators has proven promising as a straightforward, inexpensive fabrication approach. Given the variety of emitters that can easily be incorporated within NFES polymer fibers, the biocompatibility of PVA, and the spatial precision associated with the direct-write

technique, multiplexed WGM polymer fiber sensors capable of simultaneously detecting multiple analytes are within reach.

4. Conflict of Interest

There are no conflicts to declare.

5. Acknowledgement

This material is based upon work supported by the National Science Foundation under Grant No. ECCS-1406795 and the UCR CoR Grant Program. In addition, this study utilized the Analytical Chemistry Instrumentation Facility, the Institute for Integrative Genome Biology at UC Riverside, Winston Chung Global Energy Center and Ming Chi University of Technology.

6. Notes and References

1 V. Duong Ta, R. Chen, L. Ma, Y. Jun Ying and H. Dong Sun, *Laser Photonics Rev.*, 2013, **7**, 133–139.

2 T. Grossmann, S. Schleede, M. Hauser, M. B. Christiansen, C. Vannahme, C. Eschenbaum, S. Klinkhammer, T. Beck, J. Fuchs, G. U. Nienhaus, U. Lemmer, A. Kristensen, T. Mappes and H. Kalt, *Appl. Phys. Lett.*, 2010, **97**, 1–4.

3 Y. Wang, V. D. Ta, K. S. Leck, B. H. I. Tan, Z. Wang, T. He, C. D. Ohl, H. V. Demir and H. Sun, *Nano Lett.*, 2017, **17**, 2640–2646.

4 T. Wienhold, S. Kraemmer, S. F. Wondimu, T. Siegle, U. Bog, U. Weinzierl, S. Schmidt, H. Becker, H. Kalt, T. Mappes, S. Koeber and C. Koos, *Lab Chip*, 2015, **15**, 3800–3806.

5 X. F. Jiang, C. L. Zou, L. Wang, Q. Gong and Y. F. Xiao, *Laser Photonics Rev.*, 2016, **10**, 40–61.

6 V. D. Ta, R. Chen and H. Sun, *Adv. Opt. Mater.*, 2014, **2**, 220–225.

7 H. Choi and A. M. Armani, *Opt. Lett.*, 2018, **43**, 2949–2952.

8 A. A. Savchenkov, A. B. Matsko, V. S. Ilchenko, I. Solomatine, D. Seidel and L. Maleki, *Phys. Rev. Lett.*, 2008, **101**, 093902.

9 A. A. Savchenkov, W. Liang, V. Ilchenko, A. Matsko and L. Maleki, *IEEE J. Sel. Top. Quantum Electron.*, 2018, **24**, 2900111.

10 R. Bischler, M. Olszyna, M. Himmelhaus and L. Dähne, *Eur. Phys. J. Spec. Top.*, 2014, **223**, 2041–2055.

11 N. M. Hanumegowda, C. J. Stica, B. C. Patel, I. White and X. Fan, *Appl. Phys. Lett.*, 2005, **87**, 201107.

12 V. Zamora, A. Díez, M. V. Andrés and B. Gimeno, *Opt. Express*, 2007, **15**, 12011–12016.

13 V. D. Ta, R. Chen and H. D. Sun, *Sci. Rep.*, 2013, **3**, 1362.

14 X. Zhang, L. Ren, X. Wu, H. Li, L. Liu and L. Xu, *Opt. Express*, 2011, **19**, 22242–22247.

15 F. Vollmer and S. Arnold, *Nat. Methods*, 2008, **5**, 591–596.
16 M. D. Baaske, M. R. Foreman and F. Vollmer, *Nat. Nanotechnol.*, 2014, **9**, 933–939.
17 F. Vollmer, S. Arnold and D. Keng, *Proc. Natl. Acad. Sci. U. S. A.*, 2008, **105**, 20701–20704.
18 M. D. Baaske and F. Vollmer, *Nat. Photonics*, 2016, **10**, 733–739.
19 T. Siegle, M. Remmel, S. Krämmer and H. Kalt, *APL Photonics*, 2017, **2**, 096103.
20 Y. Yang, Y. Ooka, R. Thompson, J. Ward and S. N. Chormaic, *Opt. Lett.*, 2015, **41**, 8–11.
21 C. L. Linslal, M. Kailasnath, S. Mathew, T. K. Nideep, P. Radhakrishnan, V. P. N. Nampoori and C. P. G. Vallabhan, *Opt. Lett.*, 2016, **41**, 551–554.
22 G. Senthil Murugan, J. S. Wilkinson and M. N. Zervas, *Opt. Express*, 2009, **17**, 11916–11925.
23 D. Navarro-Urrios, M. Baselga, F. F. Lupi, L. L. Martín, C. Pérez-Rodríguez, V. Lavin, I. R. Martín, B. Garrido and N. E. Capuj, *J. Opt. Soc. Am. B*, 2012, **29**, 3293–3298.
24 S. Imamura, R. Watahiki, R. Miura, T. Shimada and Y. K. Kato, *Appl. Phys. Lett.*, 2013, **102**, 161102.
25 B. D. Jones, M. Oxborrow, V. N. Astratov, M. Hopkinson, A. Tahraoui, M. S. Skolnick and A. M. Fox, *Opt. InfoBase Conf. Pap.*, 2011, **18**, 3302–3307.
26 S. L. McCall, A. F. J. Levi, R. E. Slusher, S. J. Pearton and R. A. Logan, *Appl. Phys. Lett.*, 1992, **60**, 289–291.
27 E. D. Haberer, R. Sharma, C. Meier, A. R. Stonas, S. Nakamura, S. P. Denbaars and E. L. Hu, *Appl. Phys. Lett.*, 2004, **85**, 5179–5181.
28 T. Kipp, H. Welsch, C. Strelow, C. Heyn and D. Heitmann, *Phys. Rev. Lett.*, 2006, **96**, 077403.
29 K. Srinivasan, A. Stintz, S. Krishna and O. Painter, *Phys. Rev. B - Condens. Matter Mater. Phys.*, 2005, **72**, 205318.
30 A. M. Armani, A. Srinivasan and K. J. Vahala, *Nano Lett.*, 2007, **7**, 1823–1826.
31 A. François, N. Riesen, H. Ji, S. Afshar V. and T. M. Monro, *Appl. Phys. Lett.*, 2015, **106**, 031104.
32 C. Chen, L. Wan, H. Chandrahalim, J. Zhou, H. Zhang, S. Cho, T. Mei, H. Yoshioka, H. Tian, N. Nishimura, X. Fan, L. J. Guo and Y. Oki, *Opt. Express*, 2018, **26**, 233–241.
33 C. L. Linslal, S. Sebastian, S. Mathew, P. Radhakrishnan, V. P. N. Nampoori, C. P. Girijavallabhan and M. Kailasnath, *Appl. Phys. Lett.*, 2015, **106**, 131101.
34 V. R. Anand, S. Mathew, B. Samuel, P. Radhakrishnan and M. Kailasnath, *Opt. Lett.*, 2017, **42**, 2926–2929.
35 S. Yang, T. Y. K. Eugene, Y. Wang, X. Zhao, H. V. Demir and H. Sun, *Opt. Express*, 2017, **25**, 2618–2626.
36 N. Bhardwaj and S. C. Kundu, *Biotechnol. Adv.*, 2010, **28**, 325–347.
37 A. J. Das, C. Lafargue, M. Lebental, J. Zyss and K. S. Narayan, *Appl. Phys. Lett.*, 2011, **99**, 263303.
38 S. Krämmer, C. Vannahme, C. L. C. Smith, T. Grossmann, M. Jenne, S. Schierle, L. Jørgensen, I. S. Chronakis, A. Kristensen and H. Kalt, *Adv. Mater.*, 2014, **26**, 8096–8100.
39 A. Camposeo, F. Di Benedetto, R. Stabile, A. A. R. Neves, R. Cingolani and D. Pisignano, *Small*, 2009, **5**, 562–566.
40 S. Ubaid, F. Liao, S. Linghu, J. Yu and F. Gu, *Opt. Lett.*, 2018, **43**, 3128–3131.
41 S. Krämmer, F. Laye, F. Friedrich, C. Vannahme, C. L. C. Smith, A. C. Mendes, I. S. Chronakis, J. Lahann, A. Kristensen and H. Kalt, *Adv. Opt. Mater.*, 2017, **5**, 1700248.
42 D. Sun, C. Chang, S. Li and L. Lin, *Nano Lett.*, 2006, **6**, 839–842.
43 D. Di Camillo, V. Fasano, F. Ruggieri, S. Santucci, L. Lozzi, A. Camposeo and D.

Pisignano, *Nanoscale*, 2013, **5**, 11637–11642.
44 G. S. Bisht, G. Canton, A. Mirsepassi, L. Kulinsky, S. Oh, D. Dunn-Rankin and M. J. Madou, *Nano Lett.*, 2011, **11**, 1831–1837.
45 F. Yan, H. Chen, L. Zheng, W. Chen, Y. Liu and Q. Hu, *Adv. J. Food Sci. Technol.*, 2013, **5**, 1073–1078.
46 P. Gaio, F. Cavalieri, E. Chiessi, C. Soagnoli and M. K. Cowman, *J. Electrochem. Soc.*, 2019, **166**, 687–691.
47 B. Suo, X. Su, J. Wu, D. Chen, A. Wang and Z. Guo, *Mater. Chem. Phys.*, 2010, **119**, 237–242.
48 K. J. Kim, S. B. Lee and N. W. Han, *Korean J. Chem. Eng.*, 1994, **11**, 41–47.
49 A. K. Sonker, K. Rathore, R. K. Nagarale and V. Verma, *J. Polym. Environ.*, 2018, **26**, 1782–1794.
50 R. P. Shaikh, P. Kumar, Y. E. Choonara, L. C. Du Toit, V. Pillay and L. C. Toit, *Biofabrication*, 2012, **4**, 025002.
51 A. G. Destaye, C. K. Lin and C. K. Lee, *ACS Appl. Mater. Interfaces*, 2013, **5**, 4745–4752.
52 C. C. Lam, P. T. Leung and K. Young, *J. Opt. Soc. Am. B*, 1992, **9**, 1585–1592.
53 T. A. Scott, *J. Phys. Chem.*, 1946, **50**, 406–412.
54 J. H. Wendorff, S. Agarwal and A. Greiner, in *Electrospinning :Materials, Processing, and Applications*, 2012, pp. 69–104.
55 J. Pu, X. Yan, Y. Jiang, C. Chang and L. Lin, *Sensors Actuators, A Phys.*, 2010, **164**, 131–136.
56 Y. Huang, Y. Duan, Y. Ding, N. Bu, Y. Pan, N. Lu and Z. Yin, *Sci. Rep.*, 2014, **4**, 5949.
57 N. Bu, Y. Huang, X. Wang and Z. Yin, *Mater. Manuf. Process.*, 2012, **27**, 1318–1323.
58 T. Siegle, J. Kellerer, M. Bonenberger, S. Krämmer, C. Klusmann, M. Müller and H. Kalt, *Opt. Express*, 2017, **26**, 3579–3593.
59 M. Sumetsky, *Opt. Lett.*, 2011, **36**, 145–147.
60 M. Sumetsky, *Int. Conf. Transparent Opt. Networks*, 2011, Tu.B4.3.
61 F. Luan, E. Magi, T. Gong, I. Kabakova and B. J. Eggleton, *Opt. Lett.*, 2011, **36**, 4761–4763.
62 F. Xie, N. Yao, W. Fang, H. Wang, F. Gu and S. Zhuang, *Photonics Res.*, 2017, **5**, B29–B33.
63 C. Strelow, H. Rehberg, C. M. Schultz, H. Welsch, C. Heyn, D. Heitmann and T. Kipp, *Phys. Rev. Lett.*, 2008, **101**, 127403.
64 T. A. Birks, J. C. Knight and T. E. Dimmick, *IEEE Photonics Technol. Lett.*, 2000, **12**, 182–183.
65 J. Wang, T. Zhan, G. Huang, X. Cui, X. Hu and Y. Mei, *Opt. Express*, 2012, **20**, 18555–18567.
66 M. L. Gorodetsky, A. A. Savchenkov and V. S. Ilchenko, *Proc. SPIE - Int. Soc. Opt. Eng.*, 1996, **2799**, 389–391.
67 M. Borselli, T. J. Johnson and O. Painter, *Opt. Express*, 2005, **13**, 1515–1530.
68 M. Kuwata-gonokami and K. Takeda, *Opt. Mater. (Amst).*, 1998, **9**, 12–17.
69 X. Chen, K. Xie, T. Hu, X. Zhang, Y. Yang, J. Ma, J. Zhang, X. Cheng and Z. Hu, *J. Phys. D. Appl. Phys.*, 2019, **52**, 475104.
70 M. Anthamatten, S. a Letts and R. C. Cook, *Langmuir*, 2004, **20**, 6288–96.
71 V. R. Anand, S. Mathew, C. L. Linslal, P. Radhakrishnan and M. Kailasnath, *J. Lumin.*, 2019, **209**, 69–73.
72 M. R. Foreman and F. Vollmer, *Phys. Rev. Lett.*, 2015, **114**, 118001.
73 J. Zhang, J. Zhong, Y. F. Fang, J. Wang, G. S. Huang, X. G. Cui and Y. F. Mei,

Nanoscale, 2014, **6**, 13646–13650.
74 K. Scholten, X. Fan and E. T. Zellers, *Lab Chip*, 2014, **14**, 3873–3880.
75 M. Charlebois, A. Paquet, L. S. Verret, K. Boissinot, M. Boissinot, M. G. Bergeron and C. N. Allen, *Nanoscale Res. Lett.*, 2010, **5**, 524–532.
76 A. Weller, F. C. Liu, R. Dahint and M. Himmelhaus, *Appl. Phys. B Lasers Opt.*, 2008, **90**, 561–567.
77 M. Himmelhaus, S. Krishnamoorthy and A. Francois, *Sensors*, 2010, **10**, 6257–6274.
78 S. Kudo, E. Otsuka and A. Suzuki, *J. Polym. Sci. Part B Polym. Phys.*, 2010, **48**, 1978–1986.
79 K. Kamemaru, S. Usui, Y. Hirashima and A. Suzuki, *Gels*, 2018, **4**, 45.
80 K. J. Kim, S. B. Lee and N. W. Han, *Polym. J.*, 1993, **25**, 1295–1302.

7. Footnotes

†Electronic Supporting Information available

‡These authors contributed equally.